



Measurement of the $B^0-\bar{B}^0$ oscillation frequency Δm_d with the decays $B^0 \rightarrow D^- \pi^+$ and $B^0 \rightarrow J/\psi K^{*0}$

The LHCb collaboration[†]

Abstract

The $B^0-\bar{B}^0$ oscillation frequency Δm_d is measured by the LHCb experiment using a dataset corresponding to an integrated luminosity of 1.0 fb^{-1} of proton-proton collisions at $\sqrt{s} = 7 \text{ TeV}$, and is found to be $\Delta m_d = 0.5156 \pm 0.0051 \text{ (stat.)} \pm 0.0033 \text{ (syst.) ps}^{-1}$. The measurement is based on results from analyses of the decays $B^0 \rightarrow D^- \pi^+$ ($D^- \rightarrow K^+ \pi^- \pi^-$) and $B^0 \rightarrow J/\psi K^{*0}$ ($J/\psi \rightarrow \mu^+ \mu^-$, $K^{*0} \rightarrow K^+ \pi^-$) and their charge conjugated modes.

Published in Physics Letters B 719 (2013), pp. 318-325

[†]Authors are listed on the following pages.

LHCb collaboration

R. Aaij³⁸, C. Abellan Beteta^{33,n}, A. Adametz¹¹, B. Adeva³⁴, M. Adinolfi⁴³, C. Adrover⁶, A. Affolder⁴⁹, Z. Ajaltouni⁵, J. Albrecht³⁵, F. Alessio³⁵, M. Alexander⁴⁸, S. Ali³⁸, G. Alkhazov²⁷, P. Alvarez Cartelle³⁴, A.A. Alves Jr²², S. Amato², Y. Amhis³⁶, L. Anderlini^{17,f}, J. Anderson³⁷, R.B. Appleby⁵¹, O. Aquines Gutierrez¹⁰, F. Archilli^{18,35}, A. Artamonov³², M. Artuso⁵³, E. Aslanides⁶, G. Auriemma^{22,m}, S. Bachmann¹¹, J.J. Back⁴⁵, C. Baesso⁵⁴, W. Baldini¹⁶, R.J. Barlow⁵¹, C. Barschel³⁵, S. Barsuk⁷, W. Barter⁴⁴, A. Bates⁴⁸, Th. Bauer³⁸, A. Bay³⁶, J. Beddow⁴⁸, I. Bediaga¹, S. Belogurov²⁸, K. Belous³², I. Belyaev²⁸, E. Ben-Haim⁸, M. Benayoun⁸, G. Bencivenni¹⁸, S. Benson⁴⁷, J. Benton⁴³, A. Berezhnoy²⁹, R. Bernet³⁷, M.-O. Bettler⁴⁴, M. van Beuzekom³⁸, A. Bien¹¹, S. Bifani¹², T. Bird⁵¹, A. Bizzeti^{17,h}, P.M. Bjørnstad⁵¹, T. Blake³⁵, F. Blanc³⁶, C. Blanks⁵⁰, J. Blouw¹¹, S. Blusk⁵³, A. Bobrov³¹, V. Bocci²², A. Bondar³¹, N. Bondar²⁷, W. Bonivento¹⁵, S. Borghi^{48,51}, A. Borgia⁵³, T.J.V. Bowcock⁴⁹, C. Bozzi¹⁶, T. Brambach⁹, J. van den Brand³⁹, J. Bressieux³⁶, D. Brett⁵¹, M. Britsch¹⁰, T. Britton⁵³, N.H. Brook⁴³, H. Brown⁴⁹, A. Büchler-Germann³⁷, I. Burducea²⁶, A. Bursche³⁷, J. Buytaert³⁵, S. Cadeddu¹⁵, O. Callot⁷, M. Calvi^{20,j}, M. Calvo Gomez^{33,n}, A. Camboni³³, P. Campana^{18,35}, A. Carbone^{14,c}, G. Carboni^{21,k}, R. Cardinale^{19,i}, A. Cardini¹⁵, H. Carranza-Mejia⁴⁷, L. Carson⁵⁰, K. Carvalho Akiba², G. Casse⁴⁹, M. Cattaneo³⁵, Ch. Cauet⁹, M. Charles⁵², Ph. Charpentier³⁵, P. Chen^{3,36}, N. Chiapolini³⁷, M. Chrzaszcz²³, K. Ciba³⁵, X. Cid Vidal³⁴, G. Ciezarek⁵⁰, P.E.L. Clarke⁴⁷, M. Clemencic³⁵, H.V. Cliff⁴⁴, J. Closier³⁵, C. Coca²⁶, V. Coco³⁸, J. Cogan⁶, E. Cogneras⁵, P. Collins³⁵, A. Comerma-Montells³³, A. Contu^{52,15}, A. Cook⁴³, M. Coombes⁴³, G. Corti³⁵, B. Couturier³⁵, G.A. Cowan³⁶, D. Craik⁴⁵, S. Cunliffe⁵⁰, R. Currie⁴⁷, C. D'Ambrosio³⁵, P. David⁸, P.N.Y. David³⁸, I. De Bonis⁴, K. De Bruyn³⁸, S. De Capua⁵¹, M. De Cian³⁷, J.M. De Miranda¹, L. De Paula², P. De Simone¹⁸, D. Decamp⁴, M. Deckenhoff⁹, H. Degaudenzi^{36,35}, L. Del Buono⁸, C. Deplano¹⁵, D. Derkach¹⁴, O. Deschamps⁵, F. Dettori³⁹, A. Di Canto¹¹, J. Dickens⁴⁴, H. Dijkstra³⁵, P. Diniz Batista¹, M. Dogaru²⁶, F. Domingo Bonal^{33,n}, S. Donleavy⁴⁹, F. Dordei¹¹, A. Dosil Suárez³⁴, D. Dossett⁴⁵, A. Dovbnya⁴⁰, F. Dupertuis³⁶, R. Dzhelyadin³², A. Dziurda²³, A. Dzyuba²⁷, S. Easo^{46,35}, U. Egede⁵⁰, V. Egorychev²⁸, S. Eidelman³¹, D. van Eijk³⁸, S. Eisenhardt⁴⁷, R. Ekelhof⁹, L. Eklund⁴⁸, I. El Rifai⁵, Ch. Elsasser³⁷, D. Elsby⁴², A. Falabella^{14,e}, C. Färber¹¹, G. Fardell⁴⁷, C. Farinelli³⁸, S. Farry¹², V. Fave³⁶, V. Fernandez Albor³⁴, F. Ferreira Rodrigues¹, M. Ferro-Luzzi³⁵, S. Filippov³⁰, C. Fitzpatrick³⁵, M. Fontana¹⁰, F. Fontanelli^{19,i}, R. Forty³⁵, O. Francisco², M. Frank³⁵, C. Frei³⁵, M. Frosini^{17,f}, S. Furcas²⁰, A. Gallas Torreira³⁴, D. Galli^{14,c}, M. Gandelman², P. Gandini⁵², Y. Gao³, J-C. Garnier³⁵, J. Garofoli⁵³, P. Garosi⁵¹, J. Garra Tico⁴⁴, L. Garrido³³, C. Gaspar³⁵, R. Gauld⁵², E. Gersabeck¹¹, M. Gersabeck³⁵, T. Gershon^{45,35}, Ph. Ghez⁴, V. Gibson⁴⁴, V.V. Gligorov³⁵, C. Göbel⁵⁴, D. Golubkov²⁸, A. Golutvin^{50,28,35}, A. Gomes², H. Gordon⁵², M. Grabalosa Gándara³³, R. Graciani Diaz³³, L.A. Granado Cardoso³⁵, E. Graugés³³, G. Graziani¹⁷, A. Greco²⁶, E. Greening⁵², S. Gregson⁴⁴, O. Grünberg⁵⁵, B. Gui⁵³, E. Gushchin³⁰, Yu. Guz³², T. Gys³⁵, C. Hadjivasiliou⁵³, G. Haefeli³⁶, C. Haen³⁵, S.C. Haines⁴⁴, S. Hall⁵⁰, T. Hampson⁴³, S. Hansmann-Menzemer¹¹, N. Harnew⁵², S.T. Harnew⁴³, J. Harrison⁵¹, P.F. Harrison⁴⁵, T. Hartmann⁵⁵, J. He⁷, V. Heijne³⁸, K. Hennessy⁴⁹, P. Henrard⁵, J.A. Hernando Morata³⁴, E. van Herwijnen³⁵, E. Hicks⁴⁹, D. Hill⁵², M. Hoballah⁵, P. Hopchev⁴, W. Hulsbergen³⁸, P. Hunt⁵², T. Huse⁴⁹, N. Hussain⁵², D. Hutchcroft⁴⁹, D. Hynds⁴⁸, V. Iakovenko⁴¹, P. Ilten¹², J. Imong⁴³, R. Jacobsson³⁵, A. Jaeger¹¹, M. Jahjah Hussein⁵, E. Jans³⁸, F. Jansen³⁸, P. Jatton³⁶, B. Jean-Marie⁷, F. Jing³, M. John⁵², D. Johnson⁵², C.R. Jones⁴⁴, B. Jost³⁵, M. Kaballo⁹, S. Kandybei⁴⁰, M. Karacson³⁵,

T.M. Karbach³⁵, I.R. Kenyon⁴², U. Kerzel³⁵, T. Ketel³⁹, A. Keune³⁶, B. Khanji²⁰, Y.M. Kim⁴⁷,
 O. Kochebina⁷, V. Komarov^{36,29}, R.F. Koopman³⁹, P. Koppenburg³⁸, M. Korolev²⁹,
 A. Kozlinskiy³⁸, L. Kravchuk³⁰, K. Kreplin¹¹, M. Kreps⁴⁵, G. Krocker¹¹, P. Krovovny³¹,
 F. Kruse⁹, M. Kucharczyk^{20,23,j}, V. Kudryavtsev³¹, T. Kvaratskheliya^{28,35}, V.N. La Thi³⁶,
 D. Lacarrere³⁵, G. Lafferty⁵¹, A. Lai¹⁵, D. Lambert⁴⁷, R.W. Lambert³⁹, E. Lanciotti³⁵,
 G. Lanfranchi^{18,35}, C. Langenbruch³⁵, T. Latham⁴⁵, C. Lazzeroni⁴², R. Le Gac⁶,
 J. van Leerdam³⁸, J.-P. Lees⁴, R. Lefèvre⁵, A. Leflat^{29,35}, J. Lefrançois⁷, O. Leroy⁶, T. Lesiak²³,
 Y. Li³, L. Li Gioi⁵, M. Liles⁴⁹, R. Lindner³⁵, C. Linn¹¹, B. Liu³, G. Liu³⁵, J. von Loeben²⁰,
 J.H. Lopes², E. Lopez Asamar³³, N. Lopez-March³⁶, H. Lu³, J. Luisier³⁶, H. Luo⁴⁷,
 A. Mac Raghne⁴⁸, F. Machefert⁷, I.V. Machikhiliyan^{4,28}, F. Maciuc²⁶, O. Maev^{27,35}, J. Magnin¹,
 M. Maino²⁰, S. Malde⁵², G. Manca^{15,d}, G. Mancinelli⁶, N. Mangiafave⁴⁴, U. Marconi¹⁴,
 R. Märki³⁶, J. Marks¹¹, G. Martellotti²², A. Martens⁸, L. Martin⁵², A. Martín Sánchez⁷,
 M. Martinelli³⁸, D. Martinez Santos³⁵, D. Martins Tostes², A. Massafferri¹, R. Matev³⁵,
 Z. Mathe³⁵, C. Matteuzzi²⁰, M. Matveev²⁷, E. Maurice⁶, A. Mazurov^{16,30,35,e}, J. McCarthy⁴²,
 G. McGregor⁵¹, R. McNulty¹², M. Meissner¹¹, M. Merk³⁸, J. Merkel⁹, D.A. Milanes¹³,
 M.-N. Minard⁴, J. Molina Rodriguez⁵⁴, S. Monteil⁵, D. Moran⁵¹, P. Morawski²³, R. Mountain⁵³,
 I. Mous³⁸, F. Muheim⁴⁷, K. Müller³⁷, R. Muresan²⁶, B. Muryn²⁴, B. Muster³⁶,
 J. Mylroie-Smith⁴⁹, P. Naik⁴³, T. Nakada³⁶, R. Nandakumar⁴⁶, I. Nasteva¹, M. Needham⁴⁷,
 N. Neufeld³⁵, A.D. Nguyen³⁶, T.D. Nguyen³⁶, C. Nguyen-Mau^{36,o}, M. Nicol⁷, V. Niess⁵,
 N. Nikitin²⁹, T. Nikodem¹¹, A. Nomerotski^{52,35}, A. Novoselov³², A. Oblakowska-Mucha²⁴,
 V. Obraztsov³², S. Oggero³⁸, S. Ogilvy⁴⁸, O. Okhrimenko⁴¹, R. Oldeman^{15,d,35}, M. Orlandea²⁶,
 J.M. Otalora Goicochea², P. Owen⁵⁰, B.K. Pal⁵³, A. Palano^{13,b}, M. Palutan¹⁸, J. Panman³⁵,
 A. Papanestis⁴⁶, M. Pappagallo⁴⁸, C. Parkes⁵¹, C.J. Parkinson⁵⁰, G. Passaleva¹⁷, G.D. Patel⁴⁹,
 M. Patel⁵⁰, G.N. Patrick⁴⁶, C. Patrignani^{19,i}, C. Pavel-Nicorescu²⁶, A. Pazos Alvarez³⁴,
 A. Pellegrino³⁸, G. Penso^{22,l}, M. Pepe Altarelli³⁵, S. Perazzini^{14,c}, D.L. Perego^{20,j},
 E. Perez Trigo³⁴, A. Pérez-Calero Yzquierdo³³, P. Perret⁵, M. Perrin-Terrin⁶, G. Pessina²⁰,
 K. Petridis⁵⁰, A. Petrolini^{19,i}, A. Phan⁵³, E. Picatoste Olloqui³³, B. Pie Valls³³, B. Pietrzyk⁴,
 T. Pilar⁴⁵, D. Pinci²², S. Playfer⁴⁷, M. Plo Casasus³⁴, F. Polci⁸, G. Polok²³, A. Poluektov^{45,31},
 E. Polcarpo², D. Popov¹⁰, B. Popovici²⁶, C. Potterat³³, A. Powell⁵², J. Prisciandaro³⁶,
 V. Pugatch⁴¹, A. Puig Navarro³⁶, W. Qian⁴, J.H. Rademacker⁴³, B. Rakotomiaramananana³⁶,
 M.S. Rangel², I. Raniuk⁴⁰, N. Rauschmayr³⁵, G. Raven³⁹, S. Redford⁵², M.M. Reid⁴⁵,
 A.C. dos Reis¹, S. Ricciardi⁴⁶, A. Richards⁵⁰, K. Rinnert⁴⁹, V. Rives Molina³³,
 D.A. Roa Romero⁵, P. Robbe⁷, E. Rodrigues^{48,51}, P. Rodriguez Perez³⁴, G.J. Rogers⁴⁴,
 S. Roiser³⁵, V. Romanovsky³², A. Romero Vidal³⁴, J. Rouvinet³⁶, T. Ruf³⁵, H. Ruiz³³,
 G. Sabatino^{22,k}, J.J. Saborido Silva³⁴, N. Sagidova²⁷, P. Sail⁴⁸, B. Saitta^{15,d}, C. Salzmann³⁷,
 B. Sanmartin Sedes³⁴, M. Sannino^{19,i}, R. Santacesaria²², C. Santamarina Rios³⁴, R. Santinelli³⁵,
 E. Santovetti^{21,k}, M. Sapunov⁶, A. Sarti^{18,l}, C. Satriano^{22,m}, A. Satta²¹, M. Savrie^{16,e},
 P. Schaack⁵⁰, M. Schiller³⁹, H. Schindler³⁵, S. Schleich⁹, M. Schlupp⁹, M. Schmelling¹⁰,
 B. Schmidt³⁵, O. Schneider³⁶, A. Schopper³⁵, M.-H. Schune⁷, R. Schwemmer³⁵, B. Sciascia¹⁸,
 A. Sciubba^{18,l}, M. Seco³⁴, A. Semennikov²⁸, K. Senderowska²⁴, I. Sepp⁵⁰, N. Serra³⁷,
 J. Serrano⁶, P. Seyfert¹¹, M. Shapkin³², I. Shapoval^{40,35}, P. Shatalov²⁸, Y. Shcheglov²⁷,
 T. Shears^{49,35}, L. Shekhtman³¹, O. Shevchenko⁴⁰, V. Shevchenko²⁸, A. Shires⁵⁰,
 R. Silva Coutinho⁴⁵, T. Skwarnicki⁵³, N.A. Smith⁴⁹, E. Smith^{52,46}, M. Smith⁵¹, K. Sobczak⁵,
 F.J.P. Soler⁴⁸, F. Soomro^{18,35}, D. Souza⁴³, B. Souza De Paula², B. Spaan⁹, A. Sparkes⁴⁷,
 P. Spradlin⁴⁸, F. Stagni³⁵, S. Stahl¹¹, O. Steinkamp³⁷, S. Stoica²⁶, S. Stone⁵³, B. Storaci³⁸,
 M. Straticiu²⁶, U. Straumann³⁷, V.K. Subbiah³⁵, S. Swientek⁹, M. Szczekowski²⁵,

P. Szczypka^{36,35}, T. Szumlak²⁴, S. T'Jampens⁴, M. Teklishyn⁷, E. Teodorescu²⁶, F. Teubert³⁵, C. Thomas⁵², E. Thomas³⁵, J. van Tilburg¹¹, V. Tisserand⁴, M. Tobin³⁷, S. Tolck³⁹, D. Tonelli³⁵, S. Topp-Joergensen⁵², N. Torr⁵², E. Tournefier^{4,50}, S. Tourneur³⁶, M.T. Tran³⁶, A. Tsaregorodtsev⁶, P. Tsopelas³⁸, N. Tuning³⁸, M. Ubeda Garcia³⁵, A. Ukleja²⁵, D. Urner⁵¹, U. Uwer¹¹, V. Vagnoni¹⁴, G. Valenti¹⁴, R. Vazquez Gomez³³, P. Vazquez Regueiro³⁴, S. Vecchi¹⁶, J.J. Velthuis⁴³, M. Veltri^{17,g}, G. Veneziano³⁶, M. Vesterinen³⁵, B. Viaud⁷, I. Videau⁷, D. Vieira², X. Vilasis-Cardona^{33,n}, J. Visniakov³⁴, A. Vollhardt³⁷, D. Volyanskyy¹⁰, D. Voong⁴³, A. Vorobyev²⁷, V. Vorobyev³¹, C. Voß⁵⁵, H. Voss¹⁰, R. Waldi⁵⁵, R. Wallace¹², S. Wandernoth¹¹, J. Wang⁵³, D.R. Ward⁴⁴, N.K. Watson⁴², A.D. Webber⁵¹, D. Websdale⁵⁰, M. Whitehead⁴⁵, J. Wicht³⁵, D. Wiedner¹¹, L. Wiggers³⁸, G. Wilkinson⁵², M.P. Williams^{45,46}, M. Williams^{50,p}, F.F. Wilson⁴⁶, J. Wishahi⁹, M. Witek²³, W. Witzeling³⁵, S.A. Wotton⁴⁴, S. Wright⁴⁴, S. Wu³, K. Wyllie³⁵, Y. Xie^{47,35}, F. Xing⁵², Z. Xing⁵³, Z. Yang³, R. Young⁴⁷, X. Yuan³, O. Yushchenko³², M. Zangoli¹⁴, M. Zavertyaev^{10,a}, F. Zhang³, L. Zhang⁵³, W.C. Zhang¹², Y. Zhang³, A. Zhelezov¹¹, L. Zhong³, A. Zvyagin³⁵.

¹ *Centro Brasileiro de Pesquisas Físicas (CBPF), Rio de Janeiro, Brazil*

² *Universidade Federal do Rio de Janeiro (UFRJ), Rio de Janeiro, Brazil*

³ *Center for High Energy Physics, Tsinghua University, Beijing, China*

⁴ *LAPP, Université de Savoie, CNRS/IN2P3, Annecy-Le-Vieux, France*

⁵ *Clermont Université, Université Blaise Pascal, CNRS/IN2P3, LPC, Clermont-Ferrand, France*

⁶ *CPPM, Aix-Marseille Université, CNRS/IN2P3, Marseille, France*

⁷ *LAL, Université Paris-Sud, CNRS/IN2P3, Orsay, France*

⁸ *LPNHE, Université Pierre et Marie Curie, Université Paris Diderot, CNRS/IN2P3, Paris, France*

⁹ *Fakultät Physik, Technische Universität Dortmund, Dortmund, Germany*

¹⁰ *Max-Planck-Institut für Kernphysik (MPIK), Heidelberg, Germany*

¹¹ *Physikalisches Institut, Ruprecht-Karls-Universität Heidelberg, Heidelberg, Germany*

¹² *School of Physics, University College Dublin, Dublin, Ireland*

¹³ *Sezione INFN di Bari, Bari, Italy*

¹⁴ *Sezione INFN di Bologna, Bologna, Italy*

¹⁵ *Sezione INFN di Cagliari, Cagliari, Italy*

¹⁶ *Sezione INFN di Ferrara, Ferrara, Italy*

¹⁷ *Sezione INFN di Firenze, Firenze, Italy*

¹⁸ *Laboratori Nazionali dell'INFN di Frascati, Frascati, Italy*

¹⁹ *Sezione INFN di Genova, Genova, Italy*

²⁰ *Sezione INFN di Milano Bicocca, Milano, Italy*

²¹ *Sezione INFN di Roma Tor Vergata, Roma, Italy*

²² *Sezione INFN di Roma La Sapienza, Roma, Italy*

²³ *Henryk Niewodniczanski Institute of Nuclear Physics Polish Academy of Sciences, Kraków, Poland*

²⁴ *AGH University of Science and Technology, Kraków, Poland*

²⁵ *National Center for Nuclear Research (NCBJ), Warsaw, Poland*

²⁶ *Horia Hulubei National Institute of Physics and Nuclear Engineering, Bucharest-Magurele, Romania*

²⁷ *Petersburg Nuclear Physics Institute (PNPI), Gatchina, Russia*

²⁸ *Institute of Theoretical and Experimental Physics (ITEP), Moscow, Russia*

²⁹ *Institute of Nuclear Physics, Moscow State University (SINP MSU), Moscow, Russia*

³⁰ *Institute for Nuclear Research of the Russian Academy of Sciences (INR RAN), Moscow, Russia*

³¹ *Budker Institute of Nuclear Physics (SB RAS) and Novosibirsk State University, Novosibirsk, Russia*

³² *Institute for High Energy Physics (IHEP), Protvino, Russia*

³³ *Universitat de Barcelona, Barcelona, Spain*

³⁴ *Universidad de Santiago de Compostela, Santiago de Compostela, Spain*

³⁵ *European Organization for Nuclear Research (CERN), Geneva, Switzerland*

- ³⁶ *Ecole Polytechnique Fédérale de Lausanne (EPFL), Lausanne, Switzerland*
- ³⁷ *Physik-Institut, Universität Zürich, Zürich, Switzerland*
- ³⁸ *Nikhef National Institute for Subatomic Physics, Amsterdam, The Netherlands*
- ³⁹ *Nikhef National Institute for Subatomic Physics and VU University Amsterdam, Amsterdam, The Netherlands*
- ⁴⁰ *NSC Kharkiv Institute of Physics and Technology (NSC KIPT), Kharkiv, Ukraine*
- ⁴¹ *Institute for Nuclear Research of the National Academy of Sciences (KINR), Kyiv, Ukraine*
- ⁴² *University of Birmingham, Birmingham, United Kingdom*
- ⁴³ *H.H. Wills Physics Laboratory, University of Bristol, Bristol, United Kingdom*
- ⁴⁴ *Cavendish Laboratory, University of Cambridge, Cambridge, United Kingdom*
- ⁴⁵ *Department of Physics, University of Warwick, Coventry, United Kingdom*
- ⁴⁶ *STFC Rutherford Appleton Laboratory, Didcot, United Kingdom*
- ⁴⁷ *School of Physics and Astronomy, University of Edinburgh, Edinburgh, United Kingdom*
- ⁴⁸ *School of Physics and Astronomy, University of Glasgow, Glasgow, United Kingdom*
- ⁴⁹ *Oliver Lodge Laboratory, University of Liverpool, Liverpool, United Kingdom*
- ⁵⁰ *Imperial College London, London, United Kingdom*
- ⁵¹ *School of Physics and Astronomy, University of Manchester, Manchester, United Kingdom*
- ⁵² *Department of Physics, University of Oxford, Oxford, United Kingdom*
- ⁵³ *Syracuse University, Syracuse, NY, United States*
- ⁵⁴ *Pontificia Universidade Católica do Rio de Janeiro (PUC-Rio), Rio de Janeiro, Brazil, associated to ²*
- ⁵⁵ *Institut für Physik, Universität Rostock, Rostock, Germany, associated to ¹¹*
- ^a *P.N. Lebedev Physical Institute, Russian Academy of Science (LPI RAS), Moscow, Russia*
- ^b *Università di Bari, Bari, Italy*
- ^c *Università di Bologna, Bologna, Italy*
- ^d *Università di Cagliari, Cagliari, Italy*
- ^e *Università di Ferrara, Ferrara, Italy*
- ^f *Università di Firenze, Firenze, Italy*
- ^g *Università di Urbino, Urbino, Italy*
- ^h *Università di Modena e Reggio Emilia, Modena, Italy*
- ⁱ *Università di Genova, Genova, Italy*
- ^j *Università di Milano Bicocca, Milano, Italy*
- ^k *Università di Roma Tor Vergata, Roma, Italy*
- ^l *Università di Roma La Sapienza, Roma, Italy*
- ^m *Università della Basilicata, Potenza, Italy*
- ⁿ *LIFAEELS, La Salle, Universitat Ramon Llull, Barcelona, Spain*
- ^o *Hanoi University of Science, Hanoi, Viet Nam*
- ^p *Massachusetts Institute of Technology, Cambridge, MA, United States*

1 Introduction

The frequency Δm_d of oscillations between B^0 mesons and \bar{B}^0 mesons also describes the mass difference Δm_d between the physical eigenstates in the B^0 - \bar{B}^0 system, and has been measured at LEP [1], the Tevatron [2, 3], and the B factories [4, 5]. The current world average is $\Delta m_d = 0.507 \pm 0.004 \text{ ps}^{-1}$ [6], whilst the best single measurement prior to this Letter is by the Belle experiment, $\Delta m_d = 0.511 \pm 0.005 \text{ (stat.)} \pm 0.006 \text{ (syst.) ps}^{-1}$ [5]. In this document the convention $\hbar = c = 1$ is used for all units.

With increasing accuracy of the measurement of Δm_s , the counterpart of Δm_d in the B_s^0 - \bar{B}_s^0 system [7], a more precise knowledge of Δm_d becomes important, as the ratio $\Delta m_d/\Delta m_s$ together with input from lattice QCD calculations [8, 9] constrains the apex of the CKM unitarity triangle [10, 11]. Therefore, the measurement of Δm_d provides an important test of the Standard Model [12, 13]. Furthermore, Δm_d is an input parameter in the determination of $\sin 2\beta$ at LHCb [14].

This Letter presents a measurement of Δm_d , using a dataset corresponding to 1.0 fb^{-1} of pp collisions at $\sqrt{s} = 7 \text{ TeV}$, using the decay channels $B^0 \rightarrow D^- \pi^+$ ($D^- \rightarrow K^+ \pi^- \pi^-$) and $B^0 \rightarrow J/\psi K^{*0}$ ($J/\psi \rightarrow \mu^+ \mu^-$, $K^{*0} \rightarrow K^+ \pi^-$) and their charge conjugated modes.

For a measurement of Δm_d , the flavour of the B^0 meson at production and decay must be known. The flavour at decay is determined in both decay channels from the charge of the final state kaon; contributions from suppressed $B^0 \rightarrow D^+ \pi^-$ amplitudes are negligible. The determination of the flavour at production is achieved by the flavour tagging algorithms which are described in more detail in Sect. 4.

The B^0 meson is defined as unmixed (mixed) if the production flavour is equal (not equal) to the flavour at decay. With this knowledge, the oscillation frequency Δm_d of the B^0 meson can be determined using the time dependent mixing asymmetry

$$\mathcal{A}_{\text{mix}}^{\text{signal}}(t) = \frac{N_{\text{unmixed}}(t) - N_{\text{mixed}}(t)}{N_{\text{unmixed}}(t) + N_{\text{mixed}}(t)} = \cos(\Delta m_d t), \quad (1)$$

where t is the B^0 decay time and $N_{(\text{un})\text{mixed}}$ is the number of (un)mixed events.

2 Experimental setup and datasets

The LHCb detector [15] is a single-arm forward spectrometer covering the pseudorapidity range $2 < \eta < 5$, designed for the study of particles containing b or c quarks. The detector includes a high precision tracking system consisting of a silicon-strip vertex detector surrounding the pp interaction region, a large-area silicon-strip detector located upstream of a dipole magnet with a bending power of about 4 Tm, and three stations of silicon-strip detectors and straw drift-tubes placed downstream. The combined tracking system has a momentum resolution $\Delta p/p$ that varies from 0.4% at 5 GeV to 0.6% at 100 GeV, and an impact parameter (IP) resolution of 20 μm for tracks with high transverse momentum. Charged hadrons are identified using two ring-imaging Cherenkov detectors. Photon, electron and hadron candidates are identified by a calorimeter system consisting of

scintillating-pad and pre-shower detectors, an electromagnetic calorimeter and a hadronic calorimeter. Muons are identified by a system composed of alternating layers of iron and multiwire proportional chambers. The trigger consists of a hardware stage, based on information from the calorimeter and muon systems, followed by a software stage which applies a full event reconstruction.

Events including $B^0 \rightarrow D^- \pi^+$ decays are required to have tracks with high transverse momentum p_T to pass the hardware trigger. The software trigger requires a two-, three- or four-track secondary vertex with a large sum of the p_T of the tracks, significant displacement from the associated primary vertex (PV), and at least one track with $p_T > 1.7$ GeV and a large impact parameter with respect to that PV, and a good track fit. A multivariate algorithm is used for the identification of the secondary vertices [16].

Events in the decay $B^0 \rightarrow J/\psi K^{*0}$ are first required to pass a hardware trigger which selects a single muon with $p_T > 1.48$ GeV. In the subsequent software trigger [16], at least one of the final state particles is required to have $p_T > 0.8$ GeV and a large IP with respect to all PVs in the event. Finally, the tracks of two or more of the final state particles are required to form a vertex which is significantly displaced from the PVs in the event.

For the simulation studies, pp collisions are generated using PYTHIA 6.4 [17] with a specific LHCb configuration [18]. Decays of hadronic particles are described by EVTGEN [19] in which final state radiation is generated using PHOTOS [20]. The interaction of the generated particles with the detector and its response are implemented using the GEANT4 toolkit [21, 22] as described in Ref. [23].

3 Selection

The decay time t of a B^0 candidate is evaluated from the measured momenta and from a vertex fit that constrains the B^0 candidate to originate from the associated PV [24], and using $t = \ell \cdot m(B^0)/p$, with the flight distance ℓ . The associated PV is the primary vertex that is closest to the decaying B^0 meson. No mass constraints on the intermediate resonances are applied. For the calculation of the invariant mass m , no mass constraints are used in the $B^0 \rightarrow D^- \pi^+$ channel, while the J/ψ mass is constrained to the world average [6] in the analysis of the decay $B^0 \rightarrow J/\psi K^{*0}$.

All kaons, pions and muons are required to have large p_T and well reconstructed tracks and vertices. In addition to this, particle identification is used to distinguish between pion, kaon and proton tracks.

The $B^0 \rightarrow D^- \pi^+$ selection requires that the D^- reconstructed mass be in a range of ± 100 MeV around the world average [6]. Furthermore, the D^- decay vertex is required to be downstream of the PV associated to the B^0 candidate.

The sum of the D^- and π^+ p_T must be larger than 5 GeV. The B^0 candidate invariant mass must be in the interval $5000 \leq m(K^+ \pi^- \pi^- \pi^+) < 5700$ MeV. Additionally, the cosine of the pointing angle between the B^0 momentum vector and the line segment between PV and secondary vertex is required to be larger than 0.999.

Candidates are classified by a boosted decision tree (BDT) [25, 26] with the AdaBoost

algorithm [27]. The BDT is trained with $B_s^0 \rightarrow D_s^- \pi^+$ candidates with no particle ID criteria applied to the daughter pions and kaons. The cut on the BDT classifier is optimised in order to maximise the significance of the $B^0 \rightarrow D^- \pi^+$ signal. Several input variables are used: the IP significance, the flight distance perpendicular to the beam axis, the vertex quality of the B^0 and the D^- candidate, the angle between the B^0 momentum and the line segment between PV and B^0 decay vertex, the angle between the D^- momentum and the line segment between PV and the D^- decay vertex, the angle between the D^- momentum and the line segment between the B^0 decay vertex and D^- decay vertex, the IP and p_T of the π^+ track, and the angle between the π^+ momentum and the line segment between PV and B^0 decay vertex. Only B^0 candidates with a decay time $t > 0.3$ ps are accepted.

To suppress potential background from misidentified kaons in $D_s^- \rightarrow K^- K^+ \pi^-$ decays, all D^- candidates are removed if they have a daughter pion candidate that might pass a loose kaon selection and are within a ± 25 MeV mass window (the D^- mass resolution is smaller than 10 MeV) around the D_s^- mass when that pion is reconstructed under the kaon mass hypothesis.

Remaining background comes from $B^0 \rightarrow D^- \rho^+$ and $B^0 \rightarrow D^{*-} \pi^+$ decays. In both cases the final state is similar to the signal, except for an additional neutral pion that is not reconstructed. This leads to two additional peaking components with invariant masses lower than those of the signal candidates. Therefore, for the measurement of Δm_d only candidates with an invariant mass in the range $5200 \leq m < 5450$ MeV are used.

The $B^0 \rightarrow J/\psi K^{*0}$ selection requires that the K^{*0} candidate has a $p_T > 2$ GeV and $826 \leq m(K^+ \pi^-) < 966$ MeV.

The unconstrained $\mu^+ \mu^-$ invariant mass must be within ± 80 MeV of the J/ψ mass [6]. B^0 candidates are required to have a large IP with respect to other PVs in the event and the B^0 decay vertex must be significantly separated from the PV. Additionally, B^0 candidates are required to have a reconstructed decay time $t > 0.3$ ps and an invariant mass in the range $5230 \leq m(J/\psi K^+ \pi^-) < 5330$ MeV. To suppress potential background from misidentified $B_s^0 \rightarrow J/\psi \phi$ decays, all candidates are removed for which the $K^+ \pi^-$ mass is within a ± 10 MeV window around the nominal $\phi(1020)$ mass when computed under the kaon mass hypothesis for the pion. The resulting mass distributions for the two decay channels are shown in Fig. 1.

4 Flavour tagging

This analysis makes use of a combination of opposite side taggers and the same side pion tagger to determine the flavour of the B^0 meson at production. The opposite side taggers, which use decay products of the b quark not belonging to the signal decay, are described in detail in Ref. [28].

The same side pion tagger uses the charge of a pion that originates from the fragmentation process of the B^0 meson or from decays of charged excited B mesons. Pion tagging candidates are required to fulfil criteria on p_T and particle identification, as well as their

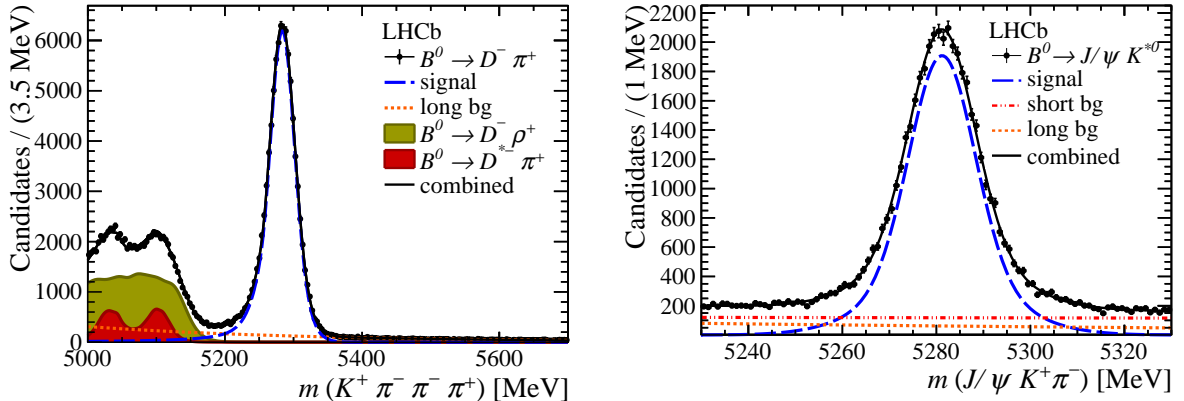


Figure 1: Distribution of the B^0 candidate mass (black points). (Left) $B^0 \rightarrow D^- \pi^+$ candidates with the invariant mass pdf as described in Sect. 6 and two additional components for the physics background taken from MC simulated events. The blue dashed line shows the fit projection of the signal, the dotted orange line corresponds to the combinatorial background, the filled areas represent the physics background, and the black solid line corresponds to the fit projection. (Right) $B^0 \rightarrow J/\psi K^{*0}$ candidates, with the results of the fits described in Sect. 6 superimposed. The blue dashed line shows the fit projection of the signal, the dotted orange line corresponds to the combinatorial background with long lifetime and the dash dotted red line shows the combinatorial background with short lifetime. The black solid line corresponds to the fit projection.

IP significance and the difference between the B^0 candidate mass and the combined mass of the B^0 candidate and the pion [29].

Depending on the tagging decision, a mixing state q is assigned to each candidate, to distinguish the unmixed ($q = +1$) from the mixed ($q = -1$). Untagged events ($q = 0$) are not used in this analysis. The tag and its predicted wrong tag probability η_c are evaluated for each event using a neural network calibrated and optimized on $B^+ \rightarrow J/\psi K^+$, $B^0 \rightarrow J/\psi K^{*0}$ and $B^0 \rightarrow D^{*-} \mu^+ \nu_\mu$ events.

To take into account a possible difference in the overall tagging performance between the calibration channels and the decay channels used in this analysis, the corrected wrong tag probability ω assigned to each event is parametrised as a linear function of η_c (the method is described and tested in Ref. [28])

$$\omega(\eta_c | p_0, p_1) = p_0 + p_1(\eta_c - \langle \eta_c \rangle), \quad (2)$$

where p_0 and p_1 are free parameters in the fit for Δm_d described in Sect. 6. In this way, uncertainties due to the overall calibration of the tagging performance are absorbed in the statistical uncertainty on Δm_d returned by the fit.

5 Decay time resolution and acceptance

The decay time resolution of the detector is around 0.05 ps [30]. This is small compared to the B^0 oscillation period of about 12 ps and does not have significant impact on the measurement of Δm_d . The resolution is accounted for by convolving a Gaussian function $G(t; \sigma_t)$, using a fixed width $\sigma_t = 0.05$ ps, with the signal probability density function (PDF) from Eq. (5). Possible systematic uncertainties introduced by the resolution are discussed in Sect. 7.

Trigger, reconstruction and selection criteria introduce efficiency effects that depend on the decay time. While these effects cancel in the asymmetry of Eq. (1) for signal events, they can be important for event samples that include background. As will be shown in Sect. 6, the only relevant background in the B^0 signal region is combinatorial in nature. For this background the asymmetry $N_{q=1}^{\text{sig}}(t) - N_{q=-1}^{\text{sig}}(t)$ is expected to cancel to first order as q has no physical meaning. Therefore,

$$\begin{aligned} \mathcal{A}_{\text{mix}}(t) &\propto \frac{(N_{q=1}^{\text{sig}}(t) + N_{q=1}^{\text{bkg}}(t)) - (N_{q=-1}^{\text{sig}}(t) + N_{q=-1}^{\text{bkg}}(t))}{(N_{q=1}^{\text{sig}}(t) + N_{q=1}^{\text{bkg}}(t)) + (N_{q=-1}^{\text{sig}}(t) + N_{q=-1}^{\text{bkg}}(t))} \\ &\propto \frac{S(t)}{S(t) + B(t)} \cos(\Delta m_d t), \end{aligned} \quad (3)$$

where $N_{q=\pm 1}^{\text{sig,bkg}}(t)$ denotes the number of unmixed or mixed signal (sig) and background (bkg) events. $S(t)$ and $B(t)$ denote the number of signal and background events as a function of the decay time. Thus, the shapes of $S(t)$ and $B(t)$ have to be known to account for the time dependent amplitude of the asymmetry function.

In the analysis of decays $B^0 \rightarrow J/\psi K^{*0}$, the decay time acceptance is determined from data, using a control sample of $B^0 \rightarrow J/\psi K^{*0}$ events that is collected without applying any of the decay time biasing selection criteria. The decay time acceptance is evaluated in bins of t and is implemented in the fit described in Sect. 6.

In the decay $B^0 \rightarrow D^- \pi^+$ there is no control dataset that can be used to measure the decay time acceptance. From an analysis of simulated events, it is determined that the decay time acceptance can be described by the empirical function

$$\epsilon_{\text{acc}}(t|a_1, a_2) = \arctan(a_1 \exp(a_2 t)), \quad (4)$$

where the parameters a_1 and a_2 are both free in the maximum likelihood fit for Δm_d described in Sect. 6.

6 Measurement of Δm_d

The value of Δm_d is measured using a multi-dimensional extended maximum likelihood fit. The $B^0 \rightarrow D^- \pi^+$ data are described by a two component PDF in which one component describes the signal and the other describes the combinatorial background. The signal component consists of the sum of a Gaussian function and a Crystal Ball function [31]

with a common mean for the mass distribution, multiplied by a function $\mathcal{P}_{\text{sig}}^t$ to describe the decay time distribution,

$$\begin{aligned} \mathcal{P}_{\text{sig}}^t(t, q; \tau, \Delta m_d, \omega, \sigma_t, a_1, a_2) \propto \\ \left[\Theta(t - 0.3 \text{ ps}) \cdot e^{-\frac{t}{\tau}} (1 + q(1 - 2\omega(\eta_c|p_0, p_1))) \cos(\Delta m_d t) \otimes G(t; \sigma_t) \right] \\ \cdot \epsilon_{\text{acc}}(t|a_1, a_2). \end{aligned} \quad (5)$$

Here, $\Theta(t)$ is the step function, while the B^0 lifetime τ is a free fit parameter and the average decay time resolution σ_t is fixed. Other fit parameters are a_1 and a_2 from the decay time acceptance function $\epsilon_{\text{acc}}(t|a_1, a_2)$ described in Sect. 5, as well as the parameters p_0 and p_1 from the tagging calibration function $\omega(\eta_c|p_0, p_1)$ described in Sect. 4. Any B^0/\bar{B}^0 production asymmetry cancels in the mixing asymmetry function, and is neglected in this analysis.

The combinatorial background component consists of an exponential PDF describing the mass distribution and the decay time PDF

$$\begin{aligned} \mathcal{P}_{\text{bkg}}^t(t, q; \tau_{\text{bkg}}, \omega_{\text{bkg}}, \sigma_t) \propto \\ \left[\Theta(t - 0.3 \text{ ps}) \cdot e^{-\frac{t}{\tau_{\text{bkg}}}} (1 + q(1 - 2\omega_{\text{bkg}})) \otimes G(t; \sigma_t) \right]. \end{aligned} \quad (6)$$

The PDF is similar to the signal decay time PDF with Δm_d fixed to zero. The parameter ω_{bkg} allows the PDF to reflect a possible asymmetry in the number of events tagged with $q = \pm 1$ in the background. The effective lifetime τ_{bkg} of the long-lived background component is allowed to vary independently in the fit.

Possible backgrounds from misidentified or partially reconstructed decays are studied using mass templates determined from simulation. These are found to be negligible in the mass window $5200 \leq m(K^+\pi^-\pi^-\pi^+) < 5450 \text{ MeV}$ that is used in the fit (c.f. Fig. 1).

In the $B^0 \rightarrow J/\psi K^{*0}$ analysis, the signal mass distribution is modelled by a double Gaussian function with a common mean and the decay time PDF is the same as described in Eq. (5), except for the decay time acceptance $\epsilon_{\text{acc}}(t|a_1, a_2)$ that is replaced by the acceptance histogram described in Sect. 5 and has no free parameters. The mass distribution of the combinatorial background in $B^0 \rightarrow J/\psi K^{*0}$ decays is also described by an exponential function. However, the decay time distribution includes a second component of shorter lifetime to account for prompt J/ψ candidates passing the selection. The long-lived component is described by the same function as the combinatorial background in $B^0 \rightarrow D^-\pi^+$ decays as in Eq. (6), whereas the short-lived component is described by a simple exponential function. No other significant source of background is found.

The resulting values for Δm_d are $0.5178 \pm 0.0061 \text{ ps}^{-1}$ and $0.5096 \pm 0.0114 \text{ ps}^{-1}$ in the $B^0 \rightarrow D^-\pi^+$ and $B^0 \rightarrow J/\psi K^{*0}$ decay modes respectively. The fit yields $87\,724 \pm 321$ signal decays for $B^0 \rightarrow D^-\pi^+$ and $39\,148 \pm 316$ signal decays for $B^0 \rightarrow J/\psi K^{*0}$. The fit projections onto the decay time distributions are displayed in Fig. 2 and the resulting asymmetries are shown in Fig. 3.

No result for the B^0 lifetime is quoted, since it is affected by possible biases due to acceptance corrections. These acceptance effects do not influence the measurement of Δm_d .

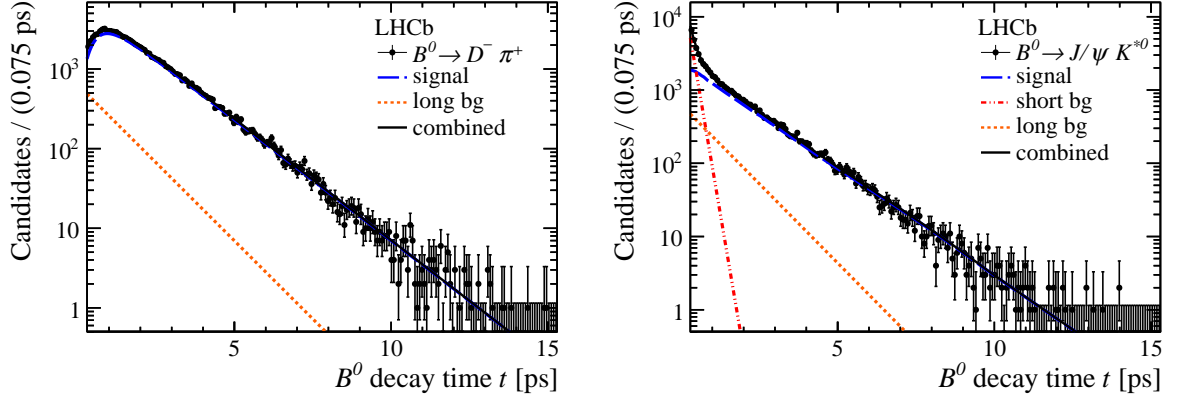


Figure 2: Distribution of the decay time (black points) for (left) $B^0 \rightarrow D^- \pi^+$ and (right) $B^0 \rightarrow J/\psi K^{*0}$ candidates. The blue dashed line shows the fit projection of the signal, the dotted orange line corresponds to the combinatorial background with long lifetime and the dash dotted red line shows the combinatorial background with short lifetime (only in the $B^0 \rightarrow J/\psi K^{*0}$ mode). The black solid line corresponds to the projection of the combined PDF.

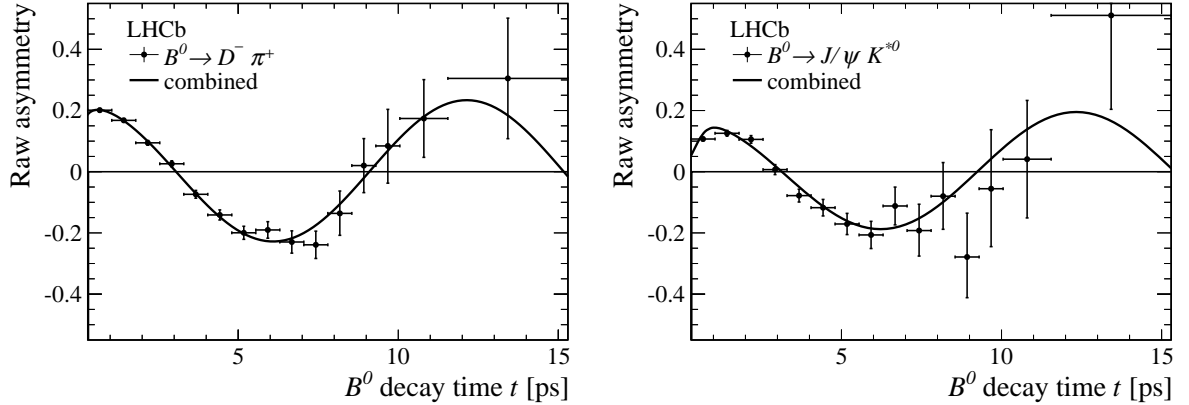


Figure 3: Raw mixing asymmetry \mathcal{A}_{mix} (black points) for (left) $B^0 \rightarrow D^- \pi^+$ and (right) $B^0 \rightarrow J/\psi K^{*0}$ candidates. The solid black line is the projection of the mixing asymmetry of the combined PDF.

7 Systematic uncertainties

As explained in Sect. 5, systematic effects due to decay time resolution are expected to be small. This is tested using samples of simulated events that are generated with decay time distributions given by the result of the fit to data and convolved with the average measured decay time resolution of 0.05 ps. The event samples are then fitted with the PDF described in Sect. 6, with the decay time resolution parameter fixed either to zero or to $\sigma_t = 0.10$ ps. The maximum observed bias on Δm_d of 0.0002 ps^{-1} is assigned as

systematic uncertainty. Systematic effects due to decay time acceptance are estimated in a similar study, generating samples of simulated events according to the nominal decay time acceptance functions described in Sect. 5. These samples are then fitted with the PDF described in Sect. 6, but neglecting the decay time acceptance function in the fit. The average observed shift of 0.0004 ps^{-1} (0.0001 ps^{-1}) in $B^0 \rightarrow D^- \pi^+$ ($B^0 \rightarrow J/\psi K^{*0}$) decays is taken as systematic uncertainty. The influence of event-by-event variation of the decay time resolution is found to be negligible.

In order to estimate systematic effects due to the parametrisation of the decay time PDFs for signal and background, an alternative parametrisation is derived with a data-driven method, using *sWeights* [32] from a fit to the mass distribution. The *sWeighted* decay time distributions for the signal and background components are then described by Gaussian kernel PDFs, which replace the exponential terms of the decay time PDF. This leads to a description of the data which is independent of a model for the decay time and its acceptance, that can be used to fit for Δm_d . The resulting shifts of 0.0037 ps^{-1} (0.0022 ps^{-1}) in the decay $B^0 \rightarrow D^- \pi^+$ ($B^0 \rightarrow J/\psi K^{*0}$) are taken as the systematic uncertainty due to the fit model.

Uncertainties in the geometric description of the detector lead to uncertainties in the measurement of flight distances and the momenta of final state particles. From alignment measurements on the vertex detector, the relative uncertainty on the length scale is known to be smaller than 0.1%. This uncertainty translates directly into a relative systematic uncertainty on Δm_d , yielding an absolute uncertainty of 0.0005 ps^{-1} .

From measurements of biases in the reconstructed J/ψ mass in several run periods, the relative uncertainty on the uncalibrated momentum scale is measured to be smaller than 0.15%. This uncertainty, however, cancels to a large extent in the calculation of the B^0 decay time, as it affects both the reconstructed B^0 momentum and its reconstructed mass, which is dominated by the measured momenta of the final state particles. The remaining systematic uncertainty on the decay time is found to be an order of magnitude smaller than that due to the length scale and is neglected.

A summary of the systematic uncertainties can be found in Table 1. The systematic uncertainty on the combined Δm_d result is calculated using a weighted average of the combined uncorrelated uncertainties in both channels. The uncertainty on the length scale is fully correlated across the channels and therefore added after the combination.

Table 1: Systematic uncertainties on Δm_d in ps^{-1}

	$B^0 \rightarrow J/\psi K^{*0}$	$B^0 \rightarrow D^- \pi^+$
Acceptance	0.0001	0.0004
Decay time resolution	0.0002	0.0002
Fit model	0.0022	0.0037
Total uncorrelated	0.0022	0.0037
Length scale	0.0005	0.0005
Total including correlated	0.0023	0.0037

8 Conclusion

The $B^0\text{-}\bar{B}^0$ oscillation frequency Δm_d has been measured using samples of $B^0 \rightarrow D^- \pi^+$ and $B^0 \rightarrow J/\psi K^{*0}$ events collected in 1.0 fb^{-1} of pp collisions at $\sqrt{s} = 7 \text{ TeV}$ and is found to be

$$\begin{aligned}\Delta m_d(B^0 \rightarrow D^- \pi^+) &= 0.5178 \pm 0.0061 \text{ (stat.)} \pm 0.0037 \text{ (syst.) ps}^{-1} \text{ and} \\ \Delta m_d(B^0 \rightarrow J/\psi K^{*0}) &= 0.5096 \pm 0.0114 \text{ (stat.)} \pm 0.0022 \text{ (syst.) ps}^{-1}.\end{aligned}$$

The combined value for Δm_d is calculated as the weighted average of the individual results taking correlated systematic uncertainties into account

$$\Delta m_d = 0.5156 \pm 0.0051 \text{ (stat.)} \pm 0.0033 \text{ (syst.) ps}^{-1}.$$

It is currently the most precise measurement of this parameter. The relative uncertainty on Δm_d is 1.2%, where it is around 0.6% for Δm_s [7]. Thus, the uncertainty on the ratio $\Delta m_d/\Delta m_s$ is dominated by Δm_d . As the systematic uncertainties in the Δm_d and Δm_s measurements are small, the error on the ratio can be further improved with more data.

Acknowledgements

We express our gratitude to our colleagues in the CERN accelerator departments for the excellent performance of the LHC. We thank the technical and administrative staff at the LHCb institutes. We acknowledge support from CERN and from the national agencies: CAPES, CNPq, FAPERJ and FINEP (Brazil); NSFC (China); CNRS/IN2P3 and Region Auvergne (France); BMBF, DFG, HGF and MPG (Germany); SFI (Ireland); INFN (Italy); FOM and NWO (The Netherlands); SCSR (Poland); ANCS/IFA (Romania); MinES, Rosatom, RFBR and NRC “Kurchatov Institute” (Russia); MinECo, XuntaGal and GENCAT (Spain); SNSF and SER (Switzerland); NAS Ukraine (Ukraine); STFC (United Kingdom); NSF (USA). We also acknowledge the support received from the ERC under FP7. The Tier1 computing centres are supported by IN2P3 (France), KIT and BMBF (Germany), INFN (Italy), NWO and SURF (The Netherlands), PIC (Spain), GridPP (United Kingdom). We are thankful for the computing resources put at our disposal by Yandex LLC (Russia), as well as to the communities behind the multiple open source software packages that we depend on.

References

- [1] ALEPH, CDF, DELPHI, L3, OPAL and SLD collaborations, D. Abbaneo *et al.*, *Combined results on B hadron production rates, lifetimes, oscillations and semileptonic decays*, arXiv:hep-ex/0009052.
- [2] D0 collaboration, V. Abazov *et al.*, *Measurement of B^0 mixing using opposite-side flavor tagging*, Phys. Rev. **D74** (2006) 112002, arXiv:hep-ex/0609034.

- [3] CDF Collaboration, T. Affolder *et al.*, *Measurement of the $B^0-\bar{B}^0$ oscillation frequency using ℓ^-D^{*+} pairs and lepton flavor tags*, Phys. Rev. **D60** (1999) 112004, [arXiv:hep-ex/9907053](#).
- [4] BaBar collaboration, B. Aubert *et al.*, *Measurement of the \bar{B}^0 lifetime and the $B^0\bar{B}^0$ oscillation frequency using partially reconstructed $\bar{B}^0 \rightarrow D^{*+}\ell^-\bar{\nu}_\ell$ decays*, Phys. Rev. **D73** (2006) 012004, [arXiv:hep-ex/0507054](#).
- [5] Belle collaboration, K. Abe *et al.*, *Improved measurement of CP-violation parameters $\sin 2\phi_1$ and $|\lambda|$, B-meson lifetimes, and $B^0\bar{B}^0$ mixing parameter Δm_d* , Phys. Rev. **D71** (2005) 072003, [arXiv:hep-ex/0408111](#).
- [6] Particle Data Group, J. Beringer *et al.*, *Review of Particle Physics (RPP)*, Phys. Rev. **D86** (2012) 010001.
- [7] LHCb collaboration, R. Aaij *et al.*, *Measurement of the $B_s^0 - \bar{B}_s^0$ oscillation frequency Δm_s in $B_s^0 \rightarrow D_s^-(3)\pi$ decays*, Phys. Lett. **B709** (2012) 177, [arXiv:1112.4311](#).
- [8] A. Hocker, H. Lacker, S. Laplace, and F. Le Diberder, *A new approach to a global fit of the CKM matrix*, Eur. Phys. J. **C21** (2001) 225, [arXiv:hep-ph/0104062](#).
- [9] G. Buchalla, A. J. Buras, and M. E. Lautenbacher, *Weak decays beyond leading logarithms*, Rev. Mod. Phys. **68** (1996) 1125, [arXiv:hep-ph/9512380](#).
- [10] CKMfitter Group, J. Charles *et al.*, *CP violation and the CKM matrix: assessing the impact of the asymmetric B factories*, Eur. Phys. J. **C41** (2005) 1, [arXiv:hep-ph/0406184](#).
- [11] UTfit Collaboration, M. Bona *et al.*, *The unitarity triangle fit in the standard model and hadronic parameters from lattice QCD: A reappraisal after the measurements of Δm_s and $\mathcal{B}(B \rightarrow \tau\nu_\tau)$* , JHEP **0610** (2006) 081, [arXiv:hep-ph/0606167](#).
- [12] J. Urban, F. Krauss, C. Hofmann, and G. Soff, *$B^0\bar{B}^0$ mixing involving supersymmetry*, Mod. Phys. Lett. **A12** (1997) 419.
- [13] J. Urban, F. Krauss, U. Jentschura, and G. Soff, *Next-to-leading order QCD corrections for the $B^0\bar{B}^0$ mixing with an extended Higgs sector*, Nucl. Phys. **B523** (1998) 40, [arXiv:hep-ph/9710245](#).
- [14] LHCb collaboration, R. Aaij *et al.*, *Measurement of the time-dependent CP asymmetry in $B^0 \rightarrow J/\psi K_s^0$ decays*, [arXiv:1211.6093](#).
- [15] LHCb collaboration, A. A. Alves Jr. *et al.*, *The LHCb detector at the LHC*, JINST **3** (2008) S08005.
- [16] R. Aaij *et al.*, *The LHCb Trigger and its Performance*, [arXiv:1211.3055](#).

- [17] T. Sjöstrand, S. Mrenna, and P. Skands, *PYTHIA 6.4 physics and manual*, JHEP **05** (2006) 026, [arXiv:hep-ph/0603175](#).
- [18] I. Belyaev *et al.*, *Handling of the generation of primary events in GAUSS, the LHCb simulation framework*, Nuclear Science Symposium Conference Record (NSS/MIC) **IEEE** (2010) 1155.
- [19] D. J. Lange, *The EvtGen particle decay simulation package*, Nucl. Instrum. Meth. **A462** (2001) 152.
- [20] P. Golonka and Z. Was, *PHOTOS Monte Carlo: a precision tool for QED corrections in Z and W decays*, Eur. Phys. J. **C45** (2006) 97, [arXiv:hep-ph/0506026](#).
- [21] GEANT4 collaboration, J. Allison *et al.*, *Geant4 developments and applications*, IEEE Trans. Nucl. Sci. **53** (2006) 270.
- [22] GEANT4 collaboration, S. Agostinelli *et al.*, *GEANT4: a simulation toolkit*, Nucl. Instrum. Meth. **A506** (2003) 250.
- [23] M. Clemencic *et al.*, *The LHCb simulation application, GAUSS: design, evolution and experience*, J. of Phys. : Conf. Ser. **331** (2011) 032023.
- [24] W. D. Hulsbergen, *Decay chain fitting with a Kalman filter*, Nucl. Instrum. Meth. **A552** (2005) 566, [arXiv:physics.comp-ph/0503191v1](#).
- [25] L. Breiman, J. H. Friedman, R. A. Olshen, and C. J. Stone, *Classification and regression trees*, Wadsworth international group, Belmont, California, USA, 1984.
- [26] B. P. Roe *et al.*, *Boosted decision trees as an alternative to artificial neural networks for particle identification*, Nucl. Instrum. Meth. **A543** (2005) 577, [arXiv:physics/0408124](#).
- [27] R. E. Schapire and Y. Freund, *A decision-theoretic generalization of on-line learning and an application to boosting*, Jour. Comp. and Syst. Sc. **55** (1997) 119.
- [28] LHCb collaboration, R. Aaij *et al.*, *Opposite-side flavour tagging of B mesons at the LHCb experiment*, Eur. Phys. J. **C72** (2012) 2022, [arXiv:1202.4979](#).
- [29] M. Grabalosa, *Flavour tagging developments within the lhcb experiment*, CERN-THESIS-2012-075.
- [30] LHCb collaboration, R. Aaij *et al.*, *Measurement of the CP-violating phase ϕ_s in the decay $B_s^0 \rightarrow J/\psi \phi$* , Phys. Rev. Lett. **108** (2012) 101803, [arXiv:1112.3183](#).
- [31] T. Skwarnicki, *A study of the radiative cascade transitions between the Upsilon-prime and Upsilon resonances*, PhD thesis, Institute of Nuclear Physics, Krakow, 1986, DESY-F31-86-02.

- [32] M. Pivk and F. R. Le Diberder, *SPlot: a statistical tool to unfold data distributions*, Nucl. Instrum. Meth. **A555** (2005) 356, [arXiv:physics/0402083](#).